The effects of orthodontic anchor screw inserted into the femur of growth-phase or mature rats —osteoid formation, bone mineral density, collagen fiber bundles, biological apatite crystal orientation—

Tatsuro NISHIMURA[1,2], Satoru MATSUNAGA[2,3], Masaaki KASAHARA[2,4], Norio KASAHARA[2,5], Takayoshi NAKANO[6], Takuya ISHIMOTO[6], Hitoshi YAMAMOTO[5], Shinichi ABE[3] and Yasushi NISHII[1]

[1] *Department of Orthodontics, Tokyo Dental College, 2-9-18 Kandamisaki-cho, Chiyoda-ku, Tokyo 101-0061, Japan*
[2] *Oral Health Science Center, Tokyo Dental College, 2-9-18 Kandamisaki-cho, Chiyoda-ku, Tokyo 101-0061, Japan*
[3] *Department of Anatomy, Tokyo Dental College, 2-9-18 Kandamisaki-cho, Chiyoda-ku, Tokyo 101-0061, Japan*
[4] *Department of Dental Materials Science , Tokyo Dental College, 2-9-18 Kandamisaki-cho, Chiyoda-ku, Tokyo 101-0061, Japan*
[5] *Department of Histology and Developmental Biology, Tokyo Dental College, 2-9-18 Kandamisaki-cho, Chiyoda-ku, Tokyo 101-0061, Japan*
[6] *Division of Materials and Manufacturing Science, Graduate School of Engineering, Osaka University, 2-1 Yamadaoka, Suita, Osaka 565-0871, Japan*
Corresponding author, Satoru MATSUNAGA; E-mail: matsuna@tdc.ac.jp

The purpose of this study is to investigate the effect of orthodontic anchor screws (OASs) inserted into the femur of growth-phase or mature rats using histological observation and bone structure analysis. The experimental animals are growth-phase (6-week-old) or mature (25-week-old) male Wistar rats. OAS was placed into the point one-third of the femoral length from the proximal end of the femur, and the response of the surrounding bone was observed and measured. The results showed at the OAS bone interface, in growth-phase rats, bone mineral density (BMD) was reduced and the running angle of collagen fiber bundles varied significantly. In mature rats, more osteoid was observed and biological apatite (BAp) crystals showed a different orientation. It was suggested that after the insertion of OASs, bone volume and quality are decreased, but after a sufficient healing period, a new bone micro/nano structure, different from the original structure, are reconstructed.

Keywords: Orthodontic anchor screw, Osteoid, Bone mineral density, Anisotropy of collagen fiber bundles, Biological apatite crystal orientation

INTRODUCTION

Orthodontic anchor screws (OASs) are now commonly used to obtain a predictable anchorage for dental and skeletal malocclusion in the orthodontic treatment[1,2]. Early orthodontic treatment, that is orthodontic treatment for young age, is recommended for skeletal malocclusion. OASs is becoming to be applied for the early orthodontic treatment. That is effective anchorage not only adult orthodontic treatment but also early orthodontic treatment. The hybrid Hyrax expander combined with OASs expands effectively narrow maxillary dentition[3,4].

The success rate of OASs in adults is 83.3%[5], on the other hand, that in young patients is 62.5%–64.5%[6]. Generally, the main causes of OASs failure are oral bacteria, poor bone condition at the site of OASs insertion, and over loading[7]. It has been reported that active bone metabolism and low bone maturity lead to a lower success rate of OASs in young patients[8]. Motoyoshi *et al*.[6] reported that a healing period of at least 3 months after OASs insertion significantly improves the success rate of OASs use in young patients, but there is no established technique or protocol.

OASs and dental implants are basically the same in that a titanium screw is placed into the jawbone[9]. Bone strength is an important factor in the success rate of dental implants[10]. It was suggested that bone strength is highly correlated not only with bone mass but also with bone quality [including bone matrix (collagen fibers, biological apatite (BAp) crystals), calcification level] and should be considered in the treatment of bone diseases[11].

To evaluate bone structure surrounding OASs should improve the success rate in young patients. The mechanical environment of the bone surrounding the OASs and the changes in the surrounding bone structure over time brought about by the healing period need to be evaluated in order to better establish the use of OASs in young patients. In addition, it has been reported that bone remodeling can occur even at a distance from the injury[12], so histological observation of the bone surrounding the OASs should allow us to assess the extent of the effect of OASs insertion.

Therefore, the purpose of this study is to investigate the effects of OAS inserted into the femur of growth-phase or mature rats using histological observation and bone structure analysis.

MATERIALS AND METHODS

Animal experiments

The animal experiments were approved by the Institutional Animal Care and Use Committee of Tokyo Dental College (approval no. 203110). Distress was alleviated by minimizing invasiveness in accordance

Received Sep 24, 2022: Accepted Mar 6, 2023
doi:10.4012/dmj.2022-209 JOI JST.JSTAGE/dmj/2022-209

with the Animal Experiment Policy of Tokyo Dental College.

Experimental animals

The experimental animals were growth-phase (6-week-old) or mature (25-week-old) male Wistar rats (each *n*=8), which were reared in plastic cages with free access to drinking water and solid chow. These rats were purchased from Sankyo Lab Service, Tokyo, Japan. The growth-phase rats were randomly divided into two subgroups (Fig. 1). In the first subgroup, OASs were inserted in the left femur, the animals were sacrificed after a 2-week healing period, and samples were collected (growth-phase OAS 2-week group; GPOAS 2w, *n*=4). Samples were also collected from the right femur, into which no OAS had been inserted, after 2 weeks (growth-phase control 2-week group; GPC 2w, *n*=4). In the second subgroup, OASs were similarly inserted in the left femur, the animals were sacrificed after an 8-week healing period, and samples were collected (growth-phase OAS 8-week group; GPOAS 8w, *n*=4). Samples were also collected from the right femur, into which no OAS had been inserted, after 8 weeks (growth-phase control 8-week group; GPC 8w, *n*=4). The mature rats were also divided randomly into two subgroups. In the first subgroup, OASs were inserted in the left femur, the animals were sacrificed after a 2-week healing period, and samples were collected (mature OAS 2-week group; MOAS 2w, *n*=4). Samples were also collected from the right femur, into which no OAS had been inserted, after 2 weeks (mature control 2-week group; MC 2w, *n*=4). In the second subgroup, OASs were similarly inserted in the left femur, the animals were sacrificed after an 8-week healing period, and samples were collected (mature OAS 8-week group; MOAS 8w, *n*=4). Samples were also collected from the right femur, into which no OAS had been inserted, after 8 weeks (mature control 8-week group; MC 8w, *n*=4).

Experimental procedure

As the reference axes of the samples, the long axis of the rat femur was designated the X axis, the anterior-posterior direction the Y axis, and the medial-lateral direction the Z axis (Fig. 2). The animals were placed under general anesthesia by intraperitoneal administration of a combination of three anesthetics (medetomidine hydrochloride, 0.75 mg/kg, Nippon Zenyaku Kogyo, Fukushima, Japan; midazolam, 4.0 mg/kg, Sand, Tokyo, Japan; and butorphanol tartrate, 5.0 mg/kg, Meiji Seika Pharma Stocks, Tokyo, Japan). From the ventral side of the rat, a skin incision measuring approximately 20 mm was opened immediately above the femur, and the muscle layer was dissected to expose the bone. The periosteum was incised and peeled away, after which the femoral length was measured with calipers, and drilling was carried out in the Y-axis direction from above the periosteum at a point one-third of the femoral length from the proximal end where there was no muscle attachment and the bone was smooth, using a standardized drill (diameter 0.5 mm, Tamiya, Shizuoka, Japan) (Fig. 3a). A titanium alloy screw (Ti-6Al-4V, length 3 mm, diameter 1.2 mm) (Le Forte system®, Jeil Medical, Seoul, Korea) was inserted at a torque of 1.0 N/cm to a depth at which the top of the OASs thread

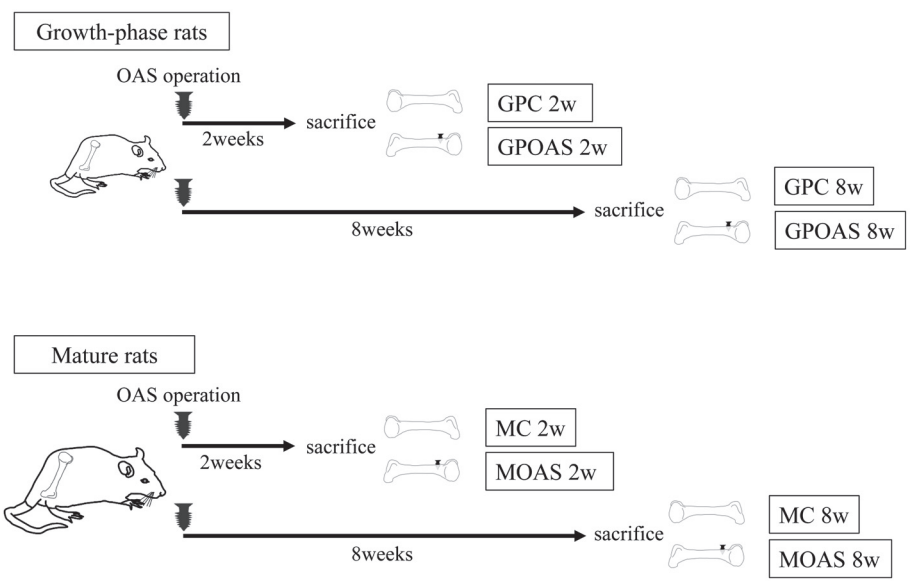

Fig. 1 Overview of the experiments.
We compared growth-phase rats with mature rats. 2-week and 8-week healing periods after OAS surgery, respectively. GPC 2w growth-phase rat control 2-week healing period, GPOAS 2w growth-phase rat OAS 2-week healing period, GPC 8w growth-phase rat control 8-week healing period, GPOAS 8w growth-phase rat OAS 8-week healing period, MC 2w mature rat control 2-week healing period, MOAS 2w growth-phase rat OAS 2-week healing period, MC 8w growth-phase rat control 8-week healing period, MOAS 8w growth-phase rat OAS 8-week healing period

was completely inserted within the cortical bone (Fig. 3b). The muscle layer and skin were then sutured with 5-0 nylon sutures to complete the operation, after which a medetomidine antagonist (0.75 mg/kg, atipamezole hydrochloride, Nippon Zenyaku Kogyo) was immediately administered intraperitoneally to maintain the rat's body temperature.

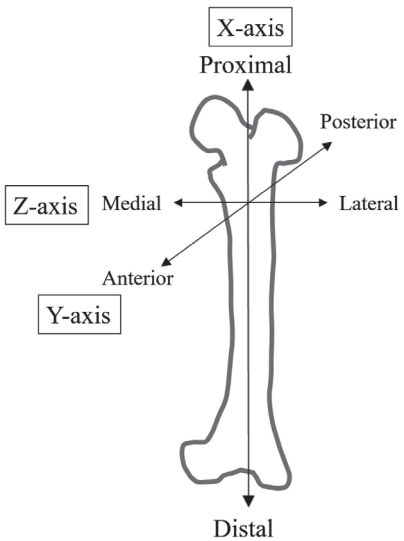

Fig. 2 Femoral coordinate axis.
As the reference axes of the samples, the long axis of the rat femur was designated the X axis, the anterior-posterior direction the Y axis, and the medial-lateral direction the Z axis.

Histological observations and osteoid measurement

OAS insertion condition was confirmed using micro CT (SCANCO μCT-50, Scanco Medical, Brüttisellen, Switzerland). The scanning conditions were tube voltage 90 kV and amplitude 44 μA. After micro CT scanning, all samples were fixed by immersion for 2 days in 10% neutral buffered formalin immediately after collection. After cutting off both ends of the samples, dehydration through graded ethanol and Villanueva osteochrome bone stain (Funakoshi, Tokyo, Japan) were performed and cleared with styrene monomer (Nisshin EM, Tokyo, Japan). The dehydrated and stained samples were subsequently embedded in unsaturated polyester resin (Rigolac, Nissin EM) based on the X-, Y-, and Z-axes. The polymerized block was sliced along the XY plane passing through the center of the OASs, using a rotary microtome (SP1600, Leica, Nussloch, Germany) with a blade width of 300 μm. It was then polished with waterproof abrasive paper (#400, #800, and #1200), and 100-μm-thick polished thin sections were prepared. These specimens were observed under a general optical microscope (Axiophoto2, Carl Zeiss, Oberkochen, Germany), and the amount of osteoid was measured as the osteoid volume per bone volume (OV/BV) and osteoid surface per bone surface (OS/BS) ratios using the image

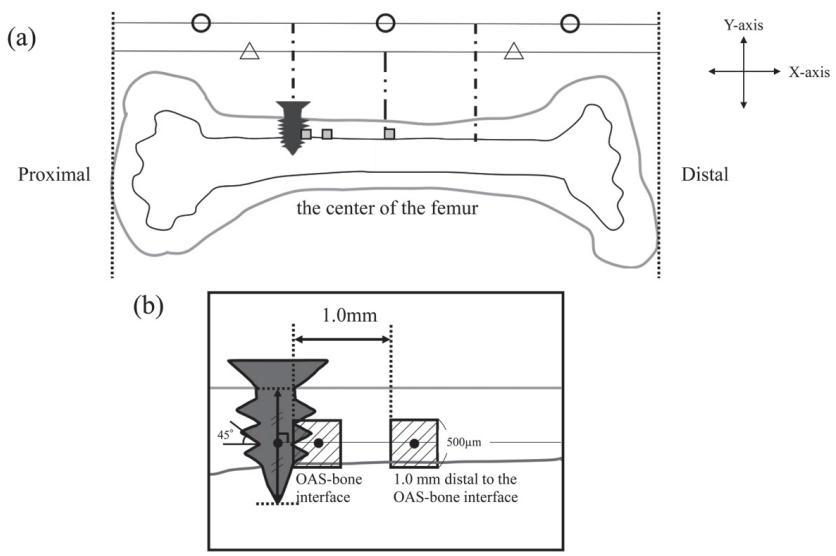

Fig. 3 OAS surgery in the femur and method of setting ROIs.
(a) The femoral length was measured with calipers and an OAS was inserted into the point one-third of the femoral length from the proximal end. (b) A line was extended distally from the center of the OAS thread in a direction perpendicular to the Y axis. Taking this perpendicular line as the height of the center of the ROIs, 500×500 μm squares were identified. Three ROIs were designated: from a point close to the OAS to the implant-bone interface; 1.0 mm distal to the OAS-bone interface; and at center of the femur.

processing software installed (Axiovision, Carl Zeiss). Haversian canals and Volkmann's canals in the cortical bone was observed under high magnification in order to measure the osteoid. White asterisks indicate uncalcified areas, black asterisk indicates calcified areas, and arrowhead indicates osteoid (Fig. 4a). The white filled area (black asterisk) indicates the OV, and the shaded area indicates the BV (Fig. 4a). The black line at the interface between the osteoid and the uncalcified area indicates the OS, and the dashed line at the interface between calcified and uncalcified areas indicates the BS (Fig. 4b).

Regions of interest (ROIs) were set for these measurements. A line was extended distally from the center of the OASs thread in a direction perpendicular to the Y axis (Fig. 3b). Taking this perpendicular line as the height of the center of the ROIs, 500×500 μm squares were identified. In addition, the OASs threads and soft tissues in the cortical bone present in the ROIs were excluded from the measurements. Three ROIs were designated: from a point close to the OAS to the OAS-bone interface; 1.0 mm distal to the OAS-bone interface; and at center of the femur (Fig. 3a). The ROIs in the control group were designated at the same three sites relative to where a hypothetical OASs would have been inserted. (GPC 2w the OAS-bone interface equivalent: A; GPOAS 2w the OAS-bone interface: B; GPOAS 2w 1.0 mm distal to the OAS-bone interface; C, GPOAS 2w center of the femur: D; GPC 8w the OAS-bone interface equivalent: E; GPOAS 8w the OAS-bone interface: F; GPOAS 8w 1.0 mm distal to the OAS-bone interface: G; GPOAS 2w center of the femur; H, MC 2w the OAS-bone interface equivalent: A'; MOAS 2w the OAS-bone interface: B'; MOAS 2w 1.0 mm distal to the OAS-bone interface: C'; MOAS 2w center of the femur: D'; MC 8w the OAS-bone interface equivalent: E'; MOAS 8w the OAS-bone interface: F'; MOAS 8w 1.0 mm distal to the OAS-bone interface; G'; MOAS 2w center of the femur: H')

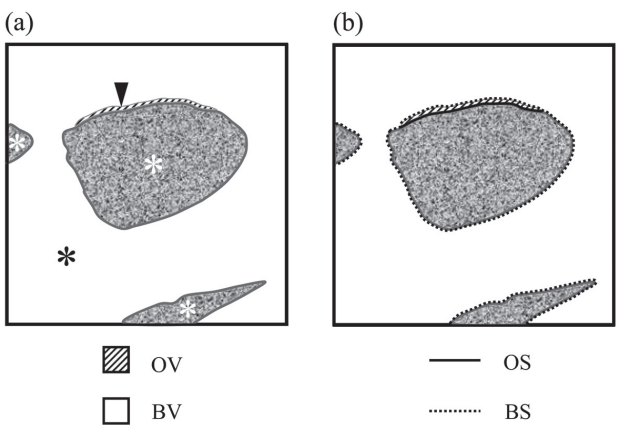

Fig. 4 Measurement method of osteoid.
(a) White asterisks indicate uncalcified areas. Black asterisk indicates calcified areas. Arrowhead indicates osteoid. The white filled area (black asterisk) indicates the OV, and the shaded area indicates the BV. (b) The black line at the interface between the osteoid and the uncalcified area indicates the OS, and the dashed line at the interface between calcified and uncalcified areas indicates the BS.

Bone mineral density (BMD) measurement

The rat femur was scanned from the proximal third containing the OAS to the center of the femur, using a microCT device. The scanning conditions were tube voltage 90 kV, amplitude 44 μA, and voxel size 14.8 μm. BMD was measured from the scanned images using the software installed in the microCT device (μCT Evaluation Program, Scanco Medical)[13].

The ROIs were the same three sites as those used for the other measurements in both the control and experimental groups.

Second harmonic generation (SHG) imaging

SHG imaging was conducted using a multiphoton confocal microscopy system (LSM 880 Airy NLO, Carl Zeiss) with an excitation laser (Chameleon Vision II, wavelengths: 680–1,080 nm; repetition rate: 80 MHz; pulse width: 140 fs; Coherent, Santa Clara, CA, USA) and an objective lens (Plan-Apochromat 10×/0.8 M27, Carl Zeiss). The excitation wavelength for collagen fiber observation was 880 nm. Software (ZEN, Carl Zeiss) was used for image capture. Collagen fiber bundles tracing and angle measurements were carried out using high-precision image analysis software (Imaris 8.4, Bitplane, Zürich, Switzerland), with reference to the Y axis as 0°.

The ROIs were the same three sites as those used for the other measurements in both the control and experimental groups.

Biological apatite (BAp) crystal orientation measurement

BAp crystal orientation was evaluated quantitatively by micro-focused X-ray diffractometry with a curved imaging plate (IP) X-ray diffractometer (XRD) D/MAX RAPIDII-CMF, Rigaku, Tokyo, Japan) incorporating two optical systems, a transmission optical system and a reflecting optical system. The radiation source was Cu-Kα radiation, and the scanning conditions were tube voltage 40 kV and tube current 30 mA. The irradiation field was determined using the optical microscope (0.6–4.8× magnification) installed in the XRD, and the incident beam became a circle with a diameter of 100 μm. For durability reasons, 100-μm-thick polished thin sections were used for the analysis.

The ROIs were the same three sites as those used for the other measurements in both the control and experimental groups (Fig. 3a).

Measurements were made with the transmission optical system in the X-axis and Y-axis orientations and with the reflecting optical system in the Z-axis orientation. From the diffraction ring image drawn on the IP with the diffracted X-ray beam, the X-ray intensity ratio of the two diffraction peaks of the (002) plane and the (310) plane was calculated using 2D date processing

software (Rigaku).

Statistical analysis

Statistical analysis was conducted with IBM SPSS Statistics (IBM, Chicago, IL, USA). The various measurements were compared using one-way analysis of variance (ANOVA) and Tukey's multiple comparison test, with $p<0.05$ regarded as significant.

RESULTS

Histological evaluation and osteoid measurement

The cortical bone surface surrounding the OAS of GPOAS 2w showed staining similar to that of bone marrow, and the cortical bone and bone marrow were irregularly intricate (Fig. 5b). Near the center of the cortical bone surrounding the OAS of GPOAS 8w, there were structures that showed staining similar to bone marrow (Fig. 5g). The GPOAS group and MOAS group showed generally similar findings, but the cortical bone at the OAS-bone interface of MOAS 8w was thicker along the OAS (Fig. 6f). Osteoid were found only at the OAS-bone interface and the region 1.0 mm distal to the OAS-bone interface in GPOAS 2w and MOAS 2w (B, C, B' and C'). A comparison between the regions showed significantly more osteoid in the region 1.0 mm distal to the OAS-bone interface (Table 1, Fig. 7). And a comparison between the GPOAS and MOAS groups showed significantly more osteoid in the MOAS group.

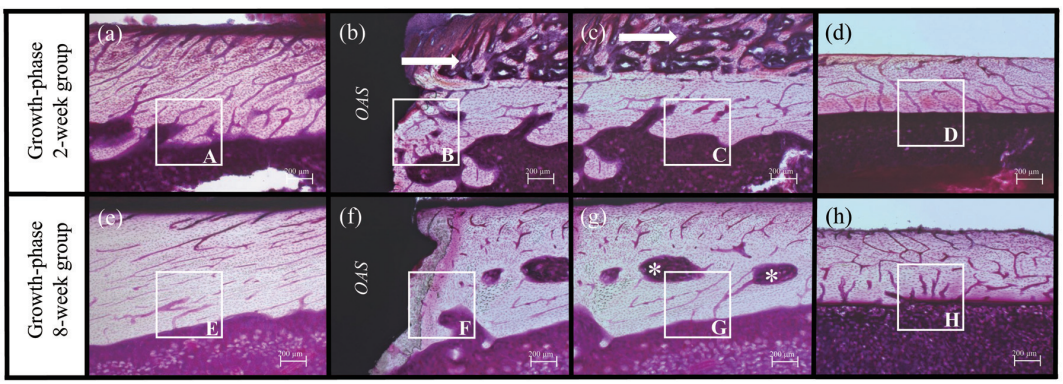

Fig. 5 Histological images of femurs of growth-phase rats.
(a) GPC 2w the OAS-bone interface equivalent, (b) GPOAS 2w the OAS-bone interface, (c) GPOAS 2w 1.0 mm distal to the OAS-bone interface, (d) GPOAS 2w the center of the femur, (e) GPC 8w the OAS-bone interface equivalent, (f) GPOAS 8w the OAS-bone interface, (g) GPOAS 8w 1.0 mm distal to the OAS-bone interface, (h) GPOAS 8w the center of the femur. White squares indicate the respective ROIs (A–H). The arrows in (b) and (c) indicated the superficial layer of cortical bone exhibited a histological appearance on that was more similar to that of the bone marrow than was the superficial layer of cortical bone in (a). The asterisks in (g) indicate bone marrow-like tissue found within the cortical bone.

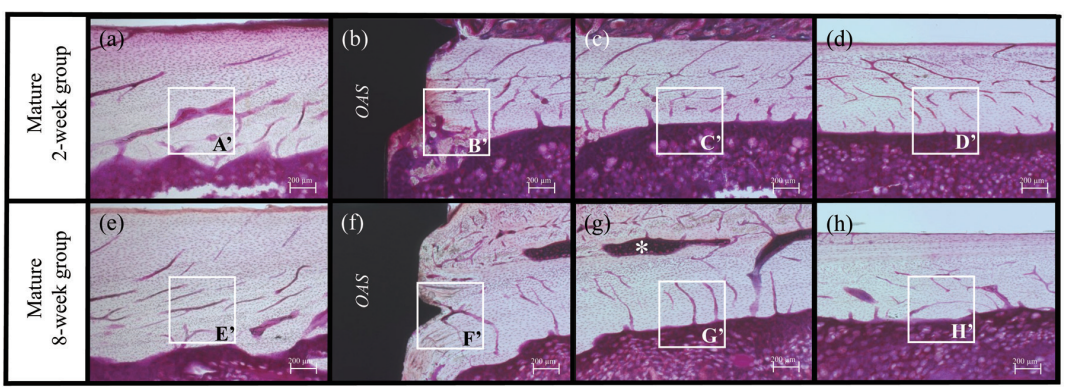

Fig. 6 Histological images of femurs of mature rats.
(a) MC 2w the OAS-bone interface equivalent, (b) MOAS 2w the OAS-bone interface, (c) MOAS 2w 1.0 mm distal to the OAS-bone interface, (d) MOAS 2w the center of the femur, (e) MC 8w the OAS-bone interface equivalent, (f) MOAS 8w the OAS-bone interface, (g) MOAS 8w 1.0 mm distal to the OAS-bone interface, (h) MOAS 8w the center of the femur. White squares indicate the respective ROIs (A'–H'). The asterisks in (g) indicate bone marrow-like tissue found within the cortical bone.

Table 1 Osteoid volume (OV) and bone volume (BV)

	OV	BV
GPC 2w region A	0.00	132,340.55
GPC 8w region E	0.00	112,569.58
MC 2w region A'	0.00	242,582.93
MC 8w region E'	0.00	194,750.05
GPOAS 2w region B	204.14	112,949.85
GPOAS 2w region C	693.37	91,771.73
MOAS 2w region B'	1,422.65	146,417.45
MOAS 2w region C'	1,839.62	144,606.01

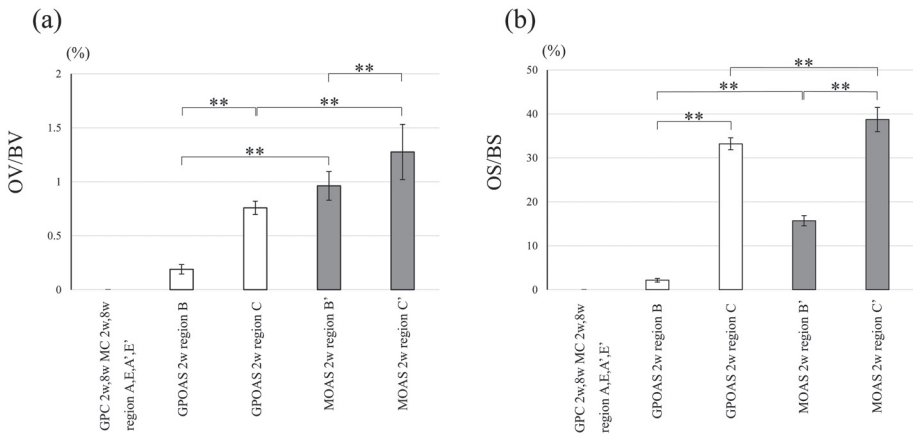

Fig. 7 Osteoid measurement.
(a) OV/BV, (%), (b) OS/BS (%). GPC 2w 8w 2w 8w region A E A' E', GPOAS 2w region B, GPOAS 2w region C, MOAS 2w region B', MOAS 2w C'. *: $p<0.05$, **: $p<0.01$

BMD Measurements

The BMD were significantly lower in the area of the OAS-bone interface compared to the 1.0 mm distal to the OAS-bone interface for 2-week groups (B, C, B' and C') (Fig. 8). The BMD of 8-week groups (GPOAS 8w and MOAS 8w) were higher than those of 2-week groups, and the difference in BMD by region was smaller. In the control groups, there was no significant difference between any of the regions (mean values±standard deviation: GPC 2w, 902.92±41.37 mgHA/ccm^3; GPC 8w, 1,033.31±27.98 mgHA/ccm^3; MC 2w, 1,059.11±31.46 mgHA/ccm^3; MC 8w, 1,072.21±25.71 mgHA/ccm^3). The values at the centers of the femurs in the experimental groups were similar to those of the control groups, with no significant differences (GPOAS 2w, 916.84±38.47 mgHA/ccm^3; GPOAS 8w, 1,029.68±8.47 mgHA/ccm^3; MOAS 2w, 1,062.21±21.50 mgHA/ccm^3; MOAS 8w, 1,066.83±17.56 mgHA/ccm^3).

SHG imaging

SHG imaging confirmed that the collagen fiber bundles running differently at the OAS-bone interface and in the region away from the OAS (Fig. 9). In all regions of the control group, away from the OAS the collagen fiber bundles tended to run almost parallel to the endosteum (almost parallel to X axis). At the OAS-bone interface in the growth-phase group (B, F), the collagen fiber bundles tended to run in a random direction. At the OAS-bone interface of MOAS 8w (F'), the collagen fiber bundles tended to run along the threads of the OAS. In the experimental groups (GPOAS 2w, GPOAS 8w, MOAS 2w, and MOAS 8w) the angle of collagen fiber bundles at the OAS-bone interface was different compared to 1.0 mm distal to the OAS-bone interface (Fig. 10). In the control group, there was no significant difference in the angle of collagen fiber bundles running in any region (GPC 2w, 97.65°±8.81°; GPC 8w, 97.10°±6.14°; MC 2w, 95.75°±4.83°; MC 8w, 94.10°±3.07°). In the experimental groups, the angle of collagen fiber bundles running in the center of femur is almost the same as that of the control group, and there is no significant difference between the control group (GPOAS 2w, 99.44°±6.52°; GPOAS 8w, 98.80°±6.20°; MOAS 2w, 95.48°±5.03°; MOAS 8w, 93.39°±2.02°). The angle of collagen fiber bundles running at the OAS-bone interface of MOAS 8w (F') was (mean±SD) 46.90 degrees (±9.50), which was

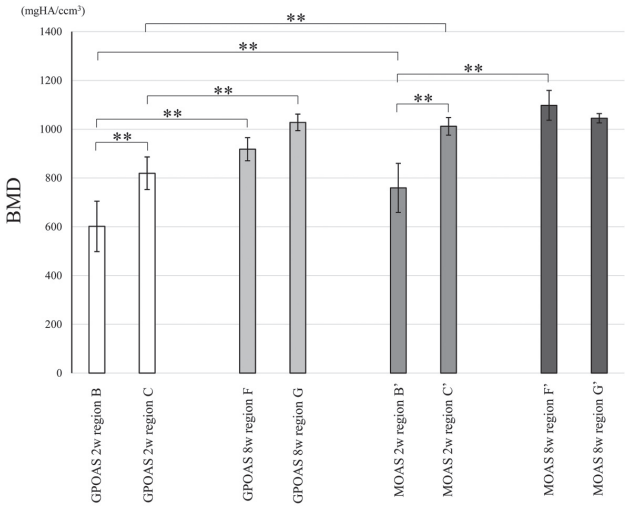

Fig. 8 BMD measurement.
GPOAS 2w region B, GPOAS 2w region C, GPOAS 8w region F, GPOAS 8w region G, MOAS 2w region B', MOAS 2w C', MOAS 8w F', MOAS 8w G'.
*: $p<0.05$, **: $p<0.01$

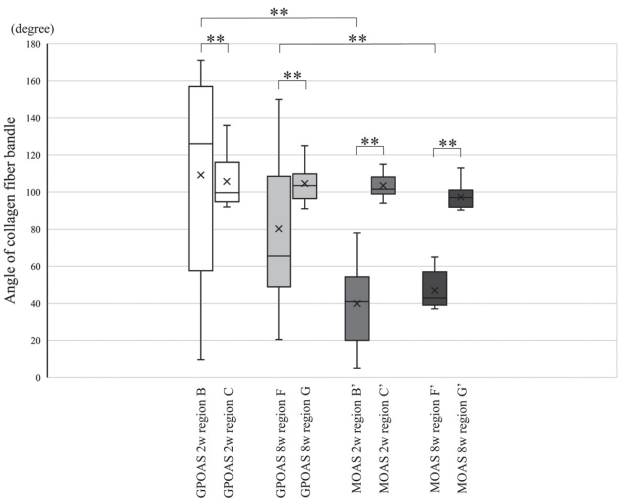

Fig. 10 Angle of collagen fiber bundles measurement.
GPOAS 2w region B, GPOAS 2w region C, GPOAS 8w region F, GPOAS 8w region G, MOAS 2w region B', MOAS 2w C', MOAS 8w F', MOAS 8w G'. *$p<0.05$, **$p<0.01$

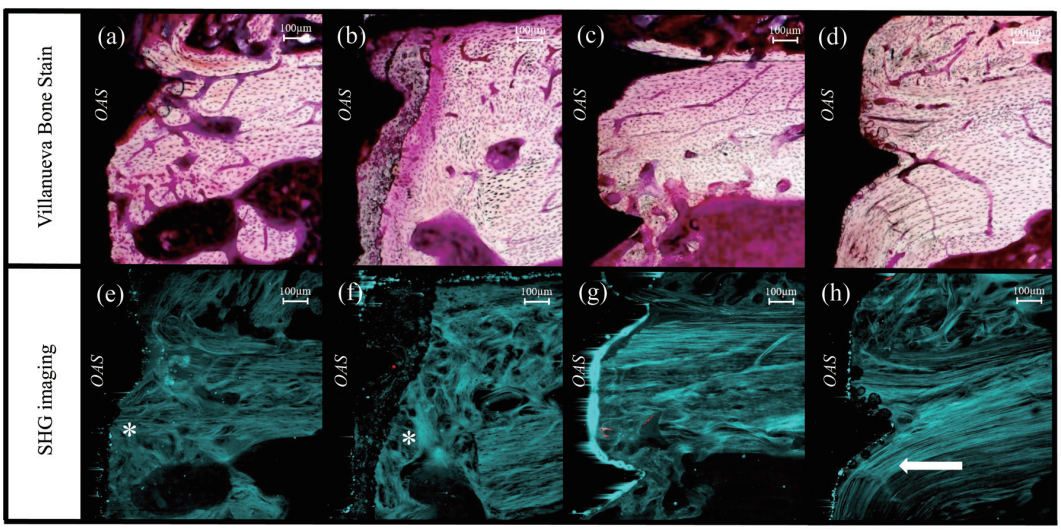

Fig. 9 The histological and SHG imaging of the OAS-bone interface in the experimental group.
(a) GPOAS 2w, (b) GPOAS 8w, (c) MOAS 2w, (d) MOAS 8w, (e) GPOAS 2w, (f) GPOAS 8w, (g) MOAS 2w, (h)MOAS 8w. Asterisks indicate collagen fiber bundles running in a random direction. Arrow indicated collagen fiber bundles running along the shape of the implant thread.

different from the control group.

BAp crystal orientation

The X-ray diffraction intensity ratio of hydroxyapatite (HAp) powder measured with the transmission optical system was 3.01, and that measured with the reflective optical system was 1.20. In all regions of the control groups, and in the regions 1.0 mm distal to the OAS-bone interface and at the center of the femur in the experimental groups, uniaxial preferred orientation in the direction of the long axis of the femur (the X-axis direction) was evident. The diffraction intensity ratio in the X-axis direction at the OAS-bone interface in experimental group (B, F, B' and F') was low and did not show preferred orientation (Figs. 11a, b). However, the Y-axis diffraction intensity ratio at the OAS-bone interface of the MOAS group was particularly high at MOAS 8w (F'), indicating a preferential orientation toward the Y-axis. No preferred orientation in the Z-axis direction was observed in any region in any group (Fig. 11c).

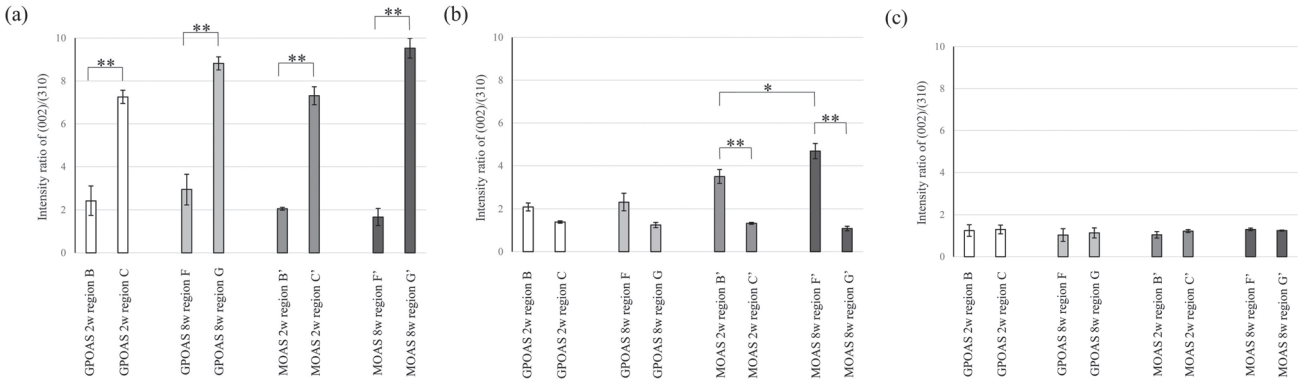

Fig. 11 Orientation of BAp in each measurement axis.
The vertical axis shows the X-ray diffraction intensity ratio calculated from the (002)/(310) peaks, and the horizontal axis shows the groups. (a) X-axis (femoral long axis) direction, (b) Y-axis (anterior-posterior) direction, (c) Z-axis (femoral long axis) direction. *: $p<0.05$, **: $p<0.01$

DISCUSSION

The cortical bone and marrow were irregularly intruded at the OAS-bone interface in GPOAS 2w and MOAS 2w, and marrow-like tissue was present near the center of the cortical bone 1.0 mm distal to the OAS-bone interface in GPOAS 8w and MOAS 8w, but no such findings were observed in the control group. This suggested that the bone surrounding the OAS was damaged by the OAS insertion, and some of the marrow was detached and moved near the center of the cortical bone as a result of further growth. Slaets *et al.*[14,15] inserted an implant into the tibia of a rabbit and reported that the appearance of new bone around the implant was observed from the second week after insertion, but a decrease in new bone was evident at the sixth week after insertion. These results are consistent with the current finding that osteoid was observed only in bone that had undergone a 2-week healing period after implant insertion. Slaets *et al.* also reported that there was a change in the nuclear morphology of osteocytes in an area 600 μm away from the implant upon implant insertion. This report shows that not only is osseointegration achieved around the implant in areas directly adjacent to the implant, but remodeling also occurs in more distant areas as a result of replacement of damaged osteocytes and bone. In the present results, osteoid was found at 2 weeks after OAS insertion in both growth-phase and mature bone, and more osteoid was found in the region 1.0 mm distal to the OAS-bone interface. This indicates that the surrounding bone dynamics are active for some time after OAS insertion, and that OAS insertion may affect not only the OAS-bone interface but also the more distal bone, replacing damaged osteocytes. Meyer *et al.*[16] reported that fracture healing in rats depends on almost all of the genes implicated in bone turnover the exhibit the same reaction to fracture healing irrespective of age. In the present study, significantly more osteoid that became secondary bone was observed in the peri-implant region in mature rats. This suggested that, even if age does not make any difference in bone turnover at the gene level, the damage caused by OAS insertion in actively growth-phase bone is unstable for the formation of osteoid, and it is possible that more osteoid was formed in mature bone where the bone condition before OAS insertion was stable.

Mori *et al.*[17] found that, when implants were inserted into the tibia of rabbits with low BMD, the BMD of peri-implant bone was significantly lower than that when implants were inserted into healthy rabbit tibia. They also reported that the bone surrounding OAS formation was delayed in rabbits with low BMD than in healthy rabbits, but that at 12 weeks post-insertion, the same amount of bone had been formed as in healthy rabbits. In the results of this study, the BMD at the OAS-bone interface was significantly decreased in growth-phase bone after 2 weeks of OAS insertion compared to mature bone, but the BMD at the OAS-bone interface was significantly increased at 8 weeks after OAS insertion. These results suggest that even if the OAS is inserted in a growth-phase bone with low BMD, the bone mass will increase with an 8-week healing period, and the OAS can be used in the same way as in a mature bone.

SHG imaging results of this study showed that collagen fiber bundles in regions entirely or mostly unaffected by OASs insertion ran almost parallel to the endosteum, whereas the courses of collagen fiber bundles at the OAS-bone interface in growth-phase bone were extremely irregular. Valente *et al.*[18] reported that implant insertion causes the collagen fiber bundles at the implant thread site to change along with the thread shape, which is a factor in the long-term success of the implant. The results of this study showed that the angle of collagen fiber bundles at the OAS-bone interface runs along the shape of the OAS thread, especially in mature bone with an 8-week healing period. These results suggest that the running of collagen fiber bundles at the OAS-bone interface is reorganized by the healing period to follow the shape of the OAS thread, which may contribute to the stability of the OAS.

BAp crystals orientation in the regions that were completely or barely affected by OAS insertion showed a uniaxial preferential orientation in the X-axis direction. This is consistent with the finding by Nakano *et al.*[19] that in cortical bone of long bones, BAp crystal orientation shows a uniaxial preferential orientation in the long axis of the bone. At the OAS-bone interface, the diffraction intensity ratio was significantly lower than that of the region that was not or hardly affected by the OAS insertion, and there was no preferential orientation in the X-axis direction (the long axis direction of the femur). This suggests that the OAS insertion disrupted the continuity of the bone and the preferential orientation in the long axis direction that existed in the femur was lost. This suggests that the OASs were inserted perpendicular to the long axis direction of the bone and that the damage of the bone around the OASs disrupted the continuity of the bone and the preferential orientation in the long axis direction that existed in the femur was lost. The results of this study showed that, at the OAS-bone interface in mature bone, the diffraction intensity ratio in the Y-axis direction increased, and a preferred orientation in this direction was evident. This result indicates that the insertion may have generated residual stress in the Y-axis direction, as pointed out by Cha *et al.*[20] and Otsu *et al.*[21].

In this study, various measurements were taken in three regions, and osteoid was found mostly in the region 1.0 mm distal to the OAS-bone interface, suggesting that there may be an effect of OAS insertion in the region away from the OAS-bone interface, but no index of OASs stability was obtained. These results suggest that there is a high risk of OASs failure in the growth-phase bone in the initial state after OAS insertion from all aspects, including the presence of osteoid, low BMD, irregular running of collagen fiber bundles, and loss of preferential orientation of BAp crystals at the OAS-bone interface. However, Wu *et al.*[22] reported that a healing period of 4 to 8 weeks is required to achieve sufficient bone strength to withstand loading after insertion of an implant in rabbit tibia. This report and the results of this study suggest that if a sufficient healing period is provided after OAS insertion, comparable bone mass and quality can be eventually achieved in both growth-phase and mature bones. This suggests that if the bone mass and bone quality of the bone surrounding the OAS increases after 8 weeks, the OASs can be used well in growing patients, and that a healing period should be allowed rather than immediate load-bearing.

CONCLUSION

The above results suggest that the OASs insertion may lead to a decrease in bone mass and quality at the OAS-bone interface especially in the growth phase. In addition, a new bone micro/nano structure that is different from the original structure after OASs insertion will reconstitute by a sufficient healing period.

Clinically, the success rate of OASs in growing patients could increase by allowing a sufficient healing period before loading.

ACKNOWLEDGMENTS

This study was supported by a research grant from the Japan Society for the Promotion of Science (contract grant number: 18K09643,17K11808) and was partly supported by a grant from the Multidisciplinary Research Center for Jaw Disease (MRCJD): Achieving Longevity and Sustainability by Comprehensive Reconstruction of Oral and Maxillofacial Functions.

REFERENCES

1) Liu Y, Yang ZJ, Zhou J, Xiong P, Wang Q, Yang Y, *et al.* Comparison of anchorage efficiency of orthodontic mini-implant and conventional anchorage reinforcement in patients requiring maximum orthodontic anchorage: A systematic review and meta-analysis. J Evid Based Dent Pract 2020; 20: 101401
2) Papadopoulous MA, Papageoorgiou SN, Zogakis IP. Clinical effectiveness of orthodontic mini-screw implants: A meta-analysis. J Dent Res 2011; 90: 969-976.
3) Garib D, Miranda F, Palomo JM, Pugliese F, Bastos JCDC, Santos AMD, *et al.* Orthopedic outcomes of hybrid and conventional Hyrax expanders: Secondary data analysis from a randomized clinical trial. Angle Orthod 2021; 91: 178-186.
4) Meyns J, Brasil DM, Mazzi-Chaves JF, Politis C, Jacobs R. The clinical outcome of skeletal anchorage in interceptive treatment (in growing patients) for class III malocclusion. Int J Oral Maxillofac Surg 2018; 47: 1003-1010.
5) Chopra S, Chakranarayan A. Clinical evaluation of immediate loading of titanium orthodontic implants. Med J Armed Forces India 2015; 71: 165-170.
6) Motoyoshi M, Matsuoka M, Shimizu N. Applications of orthodontic mini-implants to adolescents. Int J Oral Maxillofac Surg 2007; 36: 695-699.
7) Ramírez-Ossa DM, Escobar-Correa N, Ramírez-Bustamante MA, Agudelo-Suárez AA. An umbrella review of the effectiveness of temporary anchorage devices and the factors that contribute to their success or failure. J Evid Based Dent Pract 2020; 20: 101402
8) Leo M, Cerroni L, Pasquantonio G, Condò SG, Condò R. Temporary anchorage devices (TADs) in orthodontics: review of the factors that influence the clinical success rate of the mini-implants. Clin Ter 2016; 167: 70-77.
9) Motoyoshi M, Hirabayashi M, Uemura M, Shimizu N. Recommended placement torque when tightening an orthodontic mini-implant. Clin Oral Implants Res 2006; 17: 109-114.
10) Miyamoto I, Tsuboi Y, Wada E, Suwa H, Iizuka T. Influence of cortical bone thickness and implant length on implant stability at the time of surgery-Clinical, prospective, biomechanical, and imaging study. Bone 2005; 37: 776-780.
11) NIH consensus development panel on osteoporosis prevention, diagnosis, and therapy, osteoporosis prevention, diagnosis, and therapy. JAMA 2001; 285: 785-795
12) Davies JE. Understanding peri-implant endosseous healing. J Dent Educ 2003; 67: 932-949.
13) Malekipour F, Whitton RC, Lee PV. Distribution of mechanical strain in equine distal metacarpal subchondral bone: A microCT-based finite element model. Medicine Novel Tech Devices 2020; 6: 100036
14) Slaets E, Carmeliet G, Naert I, Duyck J. Early trabecular bone healing around titanium implants: A histologic study in rabbits. J Periodontol 2007; 78: 510-517.
15) Slaets E, Carmeliet Geert, Naert Ignace, Duyck J. Early

cellular responses in cortical bone healing around unloaded titanium implants: An animal study. J Periodontol 2006; 77: 1015-1024.
16) Meyer Jr RA, Desai BR, Heiner DE, Fiechtl J, Porter S, Meyer MH. Young, adult, and old rats have similar changes in mRNA expression of many skeletal genes after fracture despite delayed healing with age. J Orthop Res 2006; 24: 1933-1944.
17) Mori H, Manabe M, Kurachi Y, Nagumo M. Osseointegration of dental implants in rabbit bone with low mineral density. J Oral Maxillofac Surg 1997; 55: 351-361.
18) Valente F, Scarano A, Murmura G, Varvara G, Sinjari B, Mandelli F, *et al.* Collagen fibres orientation in the bone matrix around dental implants: Does the implant's thread design play a role? Int J Mol Sci 2021; 22: 7860
19) Nakano T, Kaibara K, Tabata Y, Nagata N, Enomoto S, Marukawa E, *et al.* Unique alignment and texture of biological apatite crystallites in typical calcified tissues analyzed by microbeam x-ray diffractometer system. Bone 2002; 31: 479-487.
20) Cha JY, Pereira MD, Smith AA, Houschyar KS, Yin X, Mouraret S, *et al.* Multiscale analyses of the bone-implant interface. J Dent Res 2015; 94: 482-490.
21) Otsu Y, Matsunaga S, Furukawa T, Kitamura K, Kasahara M, Abe S, *et al.* Structural characteristics of the bone surrounding dental implants placed into the tail-suspended mice. Int J Implant Dent 2021; 7: 89.
22) Wu J, Bai YX, Wang BK. Biomechanical and histomorphometric characterizations of osseointegration during mini-screw healing in rabbit. Angle Orthod 2009; 79: 558-563.